We are IntechOpen,
the world's leading publisher of
Open Access books
Built by scientists, for scientists

4,800
Open access books available

122,000
International authors and editors

135M
Downloads

154
Countries delivered to

Our authors are among the

TOP 1%
most cited scientists

12.2%
Contributors from top 500 universities

CLARIVATE ANALYTICS
BOOK CITATION INDEX
INDEXED

WEB OF SCIENCE™

Selection of our books indexed in the Book Citation Index
in Web of Science™ Core Collection (BKCI)

Interested in publishing with us?
Contact book.department@intechopen.com

Numbers displayed above are based on latest data collected.
For more information visit www.intechopen.com

Study of Effect of Temperature Radient on Solid Dissolution Process Under Action of Transverse Rotating Magnetic Field

Rafał Rakoczy, Marian Kordas and Stanisław Masiuk

Additional information is available at the end of the chapter

http://dx.doi.org/10.5772/51296

1. Introduction

The design, scale-up and optimization of industrial processes conducted in agitated systems require, among other, precise knowledge of the hydrodynamics, mass and heat transfer parameters and reaction kinetics. Literature data available indicate that the mass-transfer process is generally the rate-limiting step in many industrial applications. Because of the tremendous importance of mass-transfer in engineering practice, a very large number of studies have determined mass-transfer coefficients both empirically and theoretically. From the practical point of view, the agitated systems are usually employed to dissolve granular or powdered solids into a liquid solvent [3].

Transfer of the solute into the main body of the fluid occurs in the three ways, dependent upon the conditions. For an infinite stagnant fluid, transfer will be by the molecular diffusion augmented by the gradients of temperature and pressure. The natural convection currents are set up owing to the difference in density between the pure solvent and the solution. This difference in inducted flow helps to carry solute away from the interface. The third mode of transport is depended on the external effects. In this way, the forced convection closely resembles natural convection expect that the liquid flow is involved by using the external force.

One of the key aspects in the dynamic behaviour of the mass-transfer processes is the role of hydrodynamics. On a macroscopic scale, the improvement of hydrodynamic conditions can be achieved by using various techniques of mixing, vibration, rotation, pulsation and oscillation in addition to other techniques like the use of fluidization, turbulence promotes or magnetic and electric fields etc. The transverse rotating magnetic field (TRMF) is a versatile

option for enhancing several physical and chemical processes. Studies over the recent decades were focused on application of magnetic field (MF) in different areas of engineering processes [21, 22]. Static, rotating or alternating MFs might be used to augment the process intensity instead of mechanically mixing. The practical applications of TRMF are presented in the relevant literature [6, 16, 18, 23, 26, 27, 29].

Recently, TRMF are widely used to control different processes in the various engineering operations [2, 9, 10]. This kind of magnetic field induces a time-averaged azimuthal force, which drives the flow of the electrical conducting fluid in circumferential direction. According to available in technical literature, the mass-transfer during the solid dissolution to the surrounding liquid under the action of TRMF has been deliberated [21, 22]. These papers present literature survey for the applications of magnetic field (MF) and the magnetically assisted fluidization (MAF) in the mass transfer enhancement.

It should be noticed that the temperature gradient induces buoyancy-driven convective flow in the fluid. This temperature gradient has a significant practical interest to the mass transfer process. It is reported that the difference between the surface temperature of solid sample and the liquid temperature has strong influence on the dissolution process [1].

The main objective of the present study is to investigate the solid dissolution process that is induced under the action of TRMF and the gradient temperature between solid surface and liquid. According to the information available in technical literature, the usage of TRMF and gradient temperature is not theoretical and practical analyzed. The obtained experimental data are generalized by using the empirical dimensionless correlations.

2. Theoretical background

2.1. Equation of magnetic induction

The flow under the action of TRMF may be determined by taking into consideration the following magnetohydrodynamic Ohm law

$$\frac{1}{\mu_m} rot\,\bar{B} = \bar{J} \tag{1}$$

The current density $(\bar{J})$ and the total electric field current $(\bar{E})$ may be expressed as follows

$$\bar{J} = \sigma_e \left[\bar{E} + \left(\bar{w} \times \bar{B} \right) \right] \tag{2}$$

$$\bar{E} = -\bar{w} \times \bar{B} + \frac{rot\,\bar{B}}{\sigma_e \mu_m} \tag{3}$$

The general Eq.(3) may be rewritten as:

$$rot\,\bar{E} = -rot\left(\bar{w}\times\bar{B}\right) + \frac{rot\,rot\,\bar{B}}{\sigma_e\mu_m}$$ (4)

Taking into consideration the following expressions

$$\Delta\bar{B} = -rot\,rot\,\bar{B} + grad\,div\,\bar{B}$$ (5)

$$rot\,\bar{E} = -\frac{\partial\bar{B}}{\partial\tau}$$ (6)

$$div\,\bar{B} = 0$$ (7)

we obtain from the Eq.(3) the well-known advection-diffusion type relation [8, 17]

$$\frac{\partial\bar{B}}{\partial\tau} = rot\left(\bar{w}\times\bar{B}\right) + \frac{\Delta\bar{B}}{\sigma_e\mu_m}$$ (8)

The above equation (8) is also called the induction equation and it characterizes the temporal evolution of the magnetic field where

$$v_m = \frac{1}{\sigma_e\mu_m}$$ (9)

is effective diffusion coefficient (magnetic viscosity or magnetic diffusivity).

Taking into accunt the above relation, Eq. (8) may be revritten in the following form

$$\frac{\partial\bar{B}}{\partial\tau} = rot\left(\bar{w}\times\bar{B}\right) + v_m\Delta\bar{B}$$ (10)

The term, $rot\left(\bar{w}\times\bar{B}\right)$, in Eq.(8) dominates when the conductivity is large, and can be regarded as describing freezing of MF lines into the liquid. The term, $v_m\Delta\bar{B}$, in the B-field equation may be treated as a diffusion term. When the electrical conductivity, σ_e, is not too large, MF lines diffuse within the fluid.

Taking into account the below definitions of the dimensionless parameters

$$\bar{B}^* = \frac{\bar{B}}{B_0};\ \tau^* = \frac{\tau}{\tau_0};\ \bar{w}^* = \frac{\bar{w}}{w_0};\ l^* = \frac{l}{l_0};\ v_m^* = \frac{v_m}{v_{m_0}};\ rot^* = \frac{rot}{l_0^{-1}};\ \Delta^* = \frac{\Delta}{l_0^{-2}};\ \frac{\partial}{\partial\tau^*} = \frac{1}{\tau_0^{-1}}\frac{\partial}{\partial\tau}$$ (11)

we get the modified form of the relation (8)

$$\frac{B_0}{\tau_0}\left[\frac{\partial \overline{B}^*}{\partial \tau^*}\right] = \frac{w_0 B_0}{l_0}\left[rot^*\left(\overline{w}^* \times \overline{B}^*\right)\right] + \frac{v_{m_0} B_0}{l_0^2}\left[\Delta^* \overline{B}^*\right]$$

(12)

The above form of Eq. (8) may be used to examine the effect of liquid flow on the MF distribution. The non-dimensional forms of these equations may be scaled against the term $\left(\frac{v_{m_0} B_0}{l_0^2}\right)$. The dimensionless form of the equation (12) may be expressed by

$$\frac{l_0^2}{v_{m_0}\tau_0}\left[\frac{\partial \overline{B}^*}{\partial t^*}\right] = \frac{w_0 l_0}{v_{m_0}}\left[rot^*\left(\overline{w}^* \times \overline{B}^*\right)\right] + \left[\Delta^* \overline{B}^*\right]$$

(13)

This equation includes the following dimensionless groups

$$Fo_m = \frac{v_{m_0}\tau_0}{l_0^2}$$

(14)

and

$$Re_m = \frac{w_0 l_0}{v_{m_0}}$$

(15)

The magnetic Reynolds number (Re_m) is analogous to the traditional Reynolds number, describes the relative importance of advection and diffusion of the MF.

Taking into account the above definitions of the non-dimensional groups (Eqs (14) and (15)), we obtain the following general relationship of the magnetic induction equation

$$\frac{1}{Fo_m}\left[\frac{\partial \overline{B}^*}{\partial \tau^*}\right] = Re_m\left[rot^*\left(\overline{w}^* \times \overline{B}^*\right)\right] + \left[\Delta^* \overline{B}^*\right]$$

(16)

It should be noticed that the time of magnetic diffusion, τ_d, may defined as follows

$$\frac{1}{Fo_m} \sim 1 \Rightarrow \tau_0 \sim \frac{l_0^2}{v_{m_0}} \Rightarrow \tau_d = \sigma_e \mu_m l_0^2$$

(17)

Taking into account the following relation

$$rot\left(\overline{w} \times \overline{B}\right) \equiv \overline{B} \, grad \, \overline{w} - \overline{w} \, grad \, \overline{B} + \overline{w} \, div \, \overline{B} - \overline{B} \, div \, \overline{w} \qquad (18)$$

we obtain the modified form of Eq. (8)

$$\overline{w} \, grad \, \overline{B} = \frac{\Delta \overline{B}}{\sigma_e \mu_m} \Rightarrow \overline{w} \, grad \, \overline{B} = v_m \Delta \overline{B} \qquad (19)$$

The governing Eq.(19) may be rewritten in a symbolic shape which is useful in the case of the dimensionless analysis

$$\frac{w_0 B_0}{l_0}\left[\overline{w}^* \, grad^* \, \overline{B}^*\right] = \frac{v_{m_0} B_0}{l_0^2}\left[v_m^* \Delta^* \, \overline{B}^*\right] \qquad (20)$$

The above Eq.(20) admits the following relation

$$\frac{w_0 B_0}{l_0} \sim \frac{v_{m_0} B_0}{l_0^2} \qquad (21)$$

where $w_0 \equiv \omega_{TRMF} l_0$ and $\Delta^* = \dfrac{\Delta}{l_0^{-2}} \Rightarrow \Delta^* = \dfrac{\Delta}{\delta_0^{-2}}$.

An important consequence of the above expression (Eq.(21)) is that the skin depth (or the penetration depth), δ, may be given as follows

$$\frac{w_0 B_0}{l_0} \sim \frac{v_{m_0} B_0}{\delta_0^2} \Rightarrow \delta_0 \sim \sqrt{\frac{v_m l_0}{w_0}} \Rightarrow \delta = \sqrt{\frac{v_m}{\omega_{WPM}}} \qquad (22)$$

This parameter may be used to describe the well-known skin effect. From the practical point of view, this phenomenon is characterized by the so-called shielding parameter

$$S = \frac{\omega_{WPM} l_0^2}{v_m} \qquad (23)$$

This dimensionless parameter see (Eq (23)) is usually applied characterize the interaction between the MF and the electrical conductivity of liquid. The condition $S \ll 1$ means that MF is not changed by the conducting liquid. On the contrary, the condition $S \gg 1$ describes the typical skin effect which means that MF can penetrate into the highly electrically conductive liquid.

2.2. Influence of transverse rotating magnetic field on solid dissolution process

Under forced convective conditions, the mathematical description of the solid dissolution process may be described by means of the differential equation of mass balance for the component i

$$\frac{\partial \rho_i}{\partial \tau} + div\left(\rho_i \overline{w}_i\right) = \Phi_i \qquad (24)$$

where Φ_i is the mass flux of component i (the volumetric mass source of component i).

The flux density of component i $\left(\overline{J}_i\right)$ may be given by

$$\overline{J}_i = \rho_i \overline{w}_i \qquad (25)$$

The diffusion flux density is described by means of the following expression

$$\overline{J_{dyf}} = \rho_i \, dif \, \overline{w}_i \Rightarrow \overline{J_{dyf}} = \rho_i \left(\overline{w}_i - \overline{w}\right) \qquad (26)$$

The relation between $\overline{J}_i$ and $\overline{J_{dyf}}$ is defined as

$$\overline{J}_i = \overline{J_{dyf}} + \rho_i \overline{w} \Rightarrow \rho_i \overline{w}_i = \rho_i \left(\overline{w}_i - \overline{w}\right) + \rho_i \overline{w} \qquad (27)$$

Including the relation (27) in equation (24) gives the following relationship for the mass balance of component i

$$\frac{\partial \rho_i}{\partial \tau} + div\left[\overline{J_{dyf}}\right] + div\left(\rho_i \overline{w}\right) = \Phi_i \qquad (28)$$

Introducing the relation

$$div\left(\rho_i \overline{w}\right) = \rho_i \, div\left(\overline{w}\right) + \overline{w} \, grad\left(\rho_i\right) \qquad (29)$$

in Eq.(28) gives the mass balance of component i

$$\frac{\partial \rho_i}{\partial \tau} + \overline{w} \, grad\left(\rho_i\right) + \rho_i \, div\left(\overline{w}\right) + div\left[\overline{J_{dyf}}\right] = \Phi_i \qquad (30)$$

The concentration of component i may be expressed as follows

$$c_i = \frac{\rho_i}{\rho} \Rightarrow \rho_i = \rho c_i \tag{31}$$

Taking into account the above equation, we find the modified form of Eq.(30)

$$\frac{\partial(\rho c_i)}{\partial \tau} + \overline{w}\, grad(\rho c_i) + (\rho c_i) div(\overline{w}) + div\left[\overline{J_{dyf}}\right] = \Phi_i \tag{32}$$

Eq.(32) may be rewritten by

$$\frac{\partial(\rho c_i)}{\partial \tau} + \overline{w}\, grad(\rho c_i) = \rho \frac{\partial c_i}{\partial \tau} + \rho \overline{w}\, grad(c_i) + c_i \frac{\partial \rho}{\partial \tau} + c_i \overline{w}\, grad(\rho) \tag{33}$$

or

$$\rho \frac{\partial c_i}{\partial \tau} + \rho \overline{w}\, grad(c_i) + c_i \left[\frac{\partial \rho}{\partial \tau} + \overline{w}\, grad(\rho) + \rho\, div(\overline{w})\right] + div\left[\overline{J_{dyf}}\right] = \Phi_i \tag{34}$$

The term in square brackets is so-called the continuity equation and this relation may be simplified in the following form

$$\frac{\partial \rho}{\partial \tau} + \overline{w}\, grad(\rho) + \rho\, div(\overline{w}) = 0 \Rightarrow \frac{d\rho}{d\tau} + div(\rho \overline{w}) = 0 \tag{35}$$

This leads to the final expression for the mass balance of component i:

$$\rho \frac{\partial c_i}{\partial \tau} + \rho \overline{w}\, grad(c_i) + div\left[\overline{J_{dyf}}\right] = \Phi_i \tag{36}$$

The total diffusion flux density $(\overline{J_{dyf}})$ is expressed as a sum of elementary fluxes considering the concentration $(\overline{J_i}(c_i))$, temperature $(\overline{J_i}(T))$, thermodynamic pressure gradient $(\overline{J_i}(p))$, and the additional force interactions $\overline{J_i}(\overline{F})$ (e.g. forced convection as a result of fluid mixing) in the following form

$$\overline{J_{dyf}} = \overline{J_i}(c_i) + \overline{J_i}(T) + \overline{J_i}(p) + \overline{J_i}(\overline{F}) \tag{37}$$

A more useful form of this equation may be obtained by introducing the proper coefficients as follows

$$\overline{J_{dyf}} = -\rho D_i\, grad(c_i) - \rho D_i k_t\, grad(\ln t) - \rho D_i k_p\, grad(\ln p) + \rho D_i k_{\overline{F}}\, \overline{F} \tag{38}$$

Under the action of TRMF the force $\overline{F}$ may be defined as the Lorenz magnetic force $\overline{F_{em}}$. This force is acting as the driving force for the liquid rotation and it may be described by

$$\overline{F_{em}} = \overline{J} \times \overline{B} \Rightarrow \overline{F_{em}} = \left[\sigma_e E + \sigma_e\left(\overline{w} \times \overline{B}\right)\right] \times \overline{B} \tag{39}$$

The above relation may be simplified as follows (the electric field vector $\overline{E}$ is omitted)

$$\overline{F_{em}} = \left(\sigma_e\left(\overline{w} \times \overline{B}\right)\right) \times \overline{B} \tag{40}$$

The related Lorenz force to the unit of liquid mass may be rewritten in the form

$$\overline{F_{em}} = \frac{1}{\rho}\left(\sigma_e\left(\overline{w} \times \overline{B}\right)\right) \times \overline{B} \tag{41}$$

Introducing the relation Eq.(41) in Eq.(38) gives the following relationship

$$\overline{J_{dyf}} = -\rho D_i\, grad(c_i) - \rho D_i k_t\, grad(\ln t) - \rho D_i k_p\, grad(\ln p) + D_i k_{\overline{F_{em}}}\left(\left(\sigma_e\left(\overline{w} \times \overline{B}\right)\right) \times \overline{B}\right) \tag{42}$$

Taking into account the above relation (Eq.(42)) we obtain the following general relationship for the mass balance of component i

$$\frac{\partial c_i}{\partial \tau} + \overline{w}\, grad(c_i) + div\left[-D_i\, grad(c_i) - D_i k_t\, grad(\ln t) - D_i k_p\, grad(\ln p)\right] + $$
$$+ div\left[\frac{D_i k_{\overline{F_{em}}}}{\rho}\left(\left(\sigma_e\left(\overline{w} \times \overline{B}\right)\right) \times \overline{B}\right)\right] = \frac{\Phi_i}{\rho} \tag{43}$$

The obtained Eq.(43) suggests that this dependence may be simplified in the following form

$$\frac{\partial c_i}{\partial \tau} + \overline{w}\, grad(c_i) + div\left[-D_i\, grad(c_i)\right] + div\left[\frac{D_m}{\rho}\left(\left(\sigma_e\left(\overline{w} \times \overline{B}\right)\right) \times \overline{B}\right)\right] = \frac{\Phi_i}{\rho} \tag{44}$$

It should be noticed that the coefficient of magnetic diffusion D_m may be expressed as follows

$$D_m = D_i k_{\overline{F_{em}}} \tag{45}$$

This coefficient may be defined by means of the following expression

$$D_m = c_i \tau_d \Rightarrow D_m = c_i \sigma_e \mu_m l_0^2 \Rightarrow D_m = \frac{c_i l_0^2}{v_m} \tag{46}$$

Taking into consideration the above relation (Eq.(46)) we obtain the relationship

$$\frac{\partial c_i}{\partial \tau} + \overline{w}\, grad(c_i) + div\left[-D_i\, grad(c_i)\right] + div\left[\frac{c_i l_0^2}{v_m \rho}\left(\left(\sigma_e\left(\overline{w} \times \overline{B}\right)\right) \times \overline{B}\right)\right] = \frac{\Phi_i}{\rho} \tag{47}$$

The above relation (Eq.(47)) may be treated as the differential mathematical model of the solid dissolution process under the action of TRMF. The right side of this equation represents the source mass of component i

$$\Phi_i = -\frac{\beta_i\, dF_m}{dV}\left(c_i - c_r\right) \Rightarrow \Phi_i = -\left(\beta_i\right)_V\left(c_i - c_r\right) \Rightarrow \Phi_i = -\left(\beta_i\right)_V \tilde{c}_i \Rightarrow \Phi_i = \left(\beta_i\right)_V\left(-\tilde{c}_i\right) \tag{48}$$

where $\left(-\tilde{c}_i\right)$ is the driving force for the solid dissolution process.

Introducing Eq.(48) in Eq.(47), gives the following relationship

$$\frac{\partial c_i}{\partial \tau} + \overline{w}\, grad(c_i) + div\left[-D_i\, grad(c_i)\right] + div\left[\frac{c_i l_0^2}{v_m \rho}\left(\left(\sigma_e\left(\overline{w} \times \overline{B}\right)\right) \times \overline{B}\right)\right] = -\frac{\left(\beta_i\right)_V \tilde{c}_i}{\rho} \tag{49}$$

Taking into account the below definition of the dimensionless parameters

$$c_i^* = \frac{c_i}{c_{i_0}}; \tilde{c}_i^* = \frac{\tilde{c}_i}{c_{i_0}}; \overline{w}^* = \frac{\overline{w}}{w_0}; D_i^* = \frac{D_i}{D_{i_0}}; \tau^* = \frac{\tau}{\tau_0}; \mu_m^* = \frac{\mu_m}{\mu_{m_0}};$$

$$v_m^* = \frac{v_m}{v_{m_0}}; \rho^* = \frac{\rho}{\rho_0}; \overline{B}^* = \frac{\overline{B}}{B_0}; \left[\left(\beta_i\right)_V\right]^* = \frac{\left(\beta_i\right)_V}{\left[\left(\beta_i\right)_V\right]_0}; \tag{50}$$

$$div^* = \frac{div}{l_0^{-1}}; Div^* = \frac{Div}{l_0^{-1}}; grad^* = \frac{grad}{l_0^{-1}};$$

we obtain the governing Eq.(50) in a symbolic form

$$\frac{c_{i_0}}{\tau_0}\left[\frac{\partial c_i^*}{\partial \tau^*}\right] + \frac{c_{i_0} w_0}{l_0}\left[\overline{w}^*\, grad^*\left(c_i^*\right)\right] - \frac{D_{i_0} c_{i_0}}{l_0^2}\left[div^*\left[D_i^*\, grad^*\left(c_i^*\right)\right]\right] +$$

$$+\frac{c_{i_0} \sigma_{e_0} w_0 B_0^2 l_0}{v_{m_0} \rho_0}\left[div^*\left[\frac{c_i^*}{v_m^* \rho^*}\left(\left(\sigma_e^*\left(\overline{w}^* \times \overline{B}^*\right)\right) \times \overline{B}^*\right)\right]\right] = -\frac{\left[\left(\beta_i\right)_V\right]_0 c_{i_0}}{\rho_0}\left[\frac{\left[\left(\beta_i\right)_V\right]^* \tilde{c}_i^*}{\rho^*}\right] \tag{51}$$

The non-dimensional form of this equation may be scaled against the convective term $\left(\dfrac{c_{i_0} w_0}{l_0}\right)$. The dimensionless form of Eq.(51) may be given as follows

$$\frac{l_0}{\tau_0 w_0}\left[\frac{\partial c_i^*}{\partial \tau^*}\right]+\left[\overline{w}^* \, grad^*\left(c_i^*\right)\right]-\frac{D_{i_0}}{l_0 w_0}\left[div^*\left[D_i^* \, grad^*\left(c_i^*\right)\right]\right]+$$
$$+\frac{\sigma_{e_0} B_0^2 l_0^2}{\nu_{m_0}\rho_0}\left[div^*\left[\frac{c_i^*}{\nu_m^*\rho^*}\left(\left(\sigma_e^*\left(\overline{w}^* \times \overline{B}^*\right)\right)\times \overline{B}^*\right)\right]\right]=-\frac{\left[(\beta_i)_V\right]_0 l_0}{\rho_0 w_0}\left[\frac{\left[(\beta_i)_V\right]^* \tilde{c}_i^*}{\rho^*}\right] \tag{52}$$

This relation includes the following dimensionless groups characterizing the dissolution process under the action of TRM

$$\frac{l_0}{\tau_0 w_0}\Rightarrow \mathrm{S}^{-1} \tag{53}$$

$$\frac{D_{i_0}}{l_0 w_0}\Rightarrow\left(\frac{\nu}{w_0 D}\right)\left(\frac{D_{i_0}}{\nu}\right)\Rightarrow \mathrm{Re}^{-1}\mathrm{Sc}_i^{-1}\Rightarrow \mathrm{Pe}_i^{-1} \tag{54}$$

$$\frac{\sigma_{e_0} B_0^2 l_0^2}{\nu_{m_0}\rho_0}\Rightarrow\left(\frac{\sigma_{e_0} B_0^2 l_0^2}{\nu\rho_0}\right)\left(\frac{\nu}{\nu_{m_0}}\right)\Rightarrow \mathrm{Q}\,\mathrm{Pr}_m\Rightarrow \mathrm{Ha}^2\,\mathrm{Pr}_m \tag{55}$$

$$\frac{\left[(\beta_i)_V\right]_0 l_0}{\rho_0 w_0}\Rightarrow\left(\frac{\left[(\beta_i)_V\right]_0 d_p^2}{\rho_0 D_{i_0}}\right)\left(\frac{\nu}{w_0 D}\right)\left(\frac{D_{i_0}}{\nu}\right)\left(\frac{D^2}{d_s^2}\right)\Rightarrow \mathrm{Sh}\,\mathrm{Sc}^{-1}\mathrm{Re}^{-1}\left(\frac{D^2}{d_s^2}\right) \tag{56}$$

Taking into account the proposed relations (53-56), we find the following dimensionless governing equation

$$\mathrm{S}^{-1}\left[\frac{\partial c_i^*}{\partial \tau^*}\right]+\left[\overline{w}^* \, grad^*\left(c_i^*\right)\right]-\mathrm{Pe}_i^{-1}\left[div^*\left[D_i^* \, grad^*\left(c_i^*\right)\right]\right]+$$
$$+\mathrm{Ha}^2\,\mathrm{Pr}_m\left[div^*\left[\frac{c_i^*}{\nu_m^*\rho^*}\left(\left(\sigma_e^*\left(\overline{w}^* \times \overline{B}^*\right)\right)\times \overline{B}^*\right)\right]\right]=-\mathrm{Sh}\,\mathrm{Sc}^{-1}\mathrm{Re}^{-1}\left(\frac{D^2}{d_s^2}\right)\left[\frac{\left[(\beta_i)_V\right]^* \tilde{c}_i^*}{\rho^*}\right] \tag{57}$$

From the dimensionless form of Eq.(57) it follows that

$$\mathrm{Sh}\,\mathrm{Sc}^{-1}\mathrm{Re}^{-1}\left(\frac{D^2}{d_s^2}\right)\sim \mathrm{Ha}^2\,\mathrm{Pr}_m\Rightarrow \mathrm{Sh}\,\mathrm{Sc}^{-1}\sim \mathrm{Ha}^2\,\mathrm{Re}\,\mathrm{Pr}_m\left(\frac{d_s^2}{D^2}\right)\Rightarrow \mathrm{Sh}\,\mathrm{Sc}^{-1}\sim \mathrm{Ta}_m\,\mathrm{Pr}_m\left(\frac{d_s^2}{D^2}\right) \tag{58}$$

Under convective conditions a relationship for the mass-transfer similar to the relationships obtained for heat-transfer may be expected of the form [11]

$$\text{Sh} = f\left(\text{Re}, \text{Sc}\right) \tag{59}$$

The two principle dimensionless groups of relevance to mass-transfer are Sherwood and Schmidt numbers. The Sherwood number can be viewed as describing the ratio of convective to diffusive transport, and finds its counterpart in heat transfer in the form of the Nusselt number [3].

The Schmidt number is a ratio of physical parameters pertinent to the system. This dimensionless group corresponds to the Prandtl number used in heat-transfer. Moreover, this number provides a measure of the relative effectiveness of momentum and mass transport by diffusion.

Added to these two groups is the Reynolds number, which represents the ratio of convective-to-viscous momentum transport. This number determines the existence of laminar or turbulent conditions of fluid flow. For small values of the Reynolds number, viscous forces are sufficiently large relative to inertia forces. But, with increasing the Reynolds number, viscous effects become progressively less important relative to inertia effects.

Evidently, for Eq.(59) to be of practical use, it must be rendered quantitative. This may be done by assuming that the functional relation is in the following form [4, 13]

$$\text{Sh} = a_1 \text{Re}^{b_1} \text{Sc}^{c_1} \tag{60}$$

The mass-transfer coefficients in the mixed systems can be correlated by the combination of Sherwood, Reynolds and Schmidt numbers. Using the proposed relation [60], it has been found possible to correlate a host of experimental data for a wide range of operations. The coefficients of relation [60] are determined from experiment. Under forced convection conditions the relation may be expressed as follows [7]

$$\text{Sh} \sim \text{Re}^{0.5} \text{Sc}^{0.33} \tag{61}$$

The exponent upon of the Schmidt number is to be 0.33 [5, 12, 14, 19, 25] as there is some theoretical and experimental evidence for this value [24], although reported values vary from 0.56 [28] to 1.13 [15].

Mass transfer process under the TRMF conditions is very complicated and may be described by the non-dimensional Eq.(57). Use of the dimensionless Sherwood number as a function of the various non-dimensional parameters yields a description of liquid-side mass transfer, which is more general and useful. Taking into account that the magnetic Prandtl number

$Pr_m = const$ (for water$Pr_m = const$) and the ratio of diameters solid sample and diameter of container $\dfrac{d_s}{D} = idem$, the obtained relationship (see Eq.(58)) may be expressed as follows

$$Sh\,Sc^{-1} \sim Ta_m Pr_m \left(\frac{d_s^2}{D^2} \right) \Rightarrow Sh = f\left(Ta_m, Sc \right) \tag{62}$$

Basing on the considerations given above, the correlations of mass transfer process under the TRMF action have the general form

$$Sh = a_2 Ta_m{}^{b_2} Sc^{c_2} \tag{63}$$

2.3. Influence of temperature gradient on the solid dissolution controlled process

As mentioned above, the temperature gradient has strong influence on the solid dissolution process. The heat transfer from the sample to the ambient fluid may be modeled by means of the well-known Nusselt type equation.

$$Nu = f\left(Re, Pr \right) \tag{64}$$

In the present report we consider the process dissolutions described by a similar but some-what modified relationship between the dimensionless Sherwood number and the numbers which are defined the intensity of the magnetic effects in the tested experimental set-up with the TRMF generator. It should be assumed that the relationship for the heat transport under the TRMF conditions can be characterized in the following general form

$$Nu = f\left(Ta_m, Pr \right) \tag{65}$$

In order to establish the effect of all important parameters on this process in the wide range of variables data we proposed the following general relationship.

$$Nu = a_3 Ta_m{}^{b_3} Pr^{c_3} \tag{66}$$

The solid dissolution process under the action of TRMF and the gradient temperature be-tween the solid surface and the liquid may be described by means of the following equa-tions system

$$\begin{cases} Sh = a_2 Ta_m{}^{b_2} Sc^{c_2} \\ Nu = a_3 Ta_m{}^{b_3} Pr^{c_3} \end{cases} \tag{67}$$

From the above relation (Eq.(67)), the ratio of Sherwood and Nusselt numbers is given by

$$\frac{\text{Sh}}{\text{Nu}} = a_4 \text{Ta}_m{}^{b_4} \left(\frac{\text{Sc}}{\text{Pr}}\right)^{c_4} \tag{68}$$

where $a_2 \neq a_3 \wedge a_4 = \dfrac{a_2}{a_3}$; $b_2 \neq b_3 \wedge b_4 = b_2 - b_3$ and $c_2 = c_3 \wedge c_4 = 0.33$.

In the relevant literature the ratio of the Schmidt and Prandtl numbers is called as the dimensionless Lewis number (the ratio of thermal diffusivity to mass diffusivity)

$$\text{Le} = \left(\frac{\text{Sc}}{\text{Pr}}\right) \Rightarrow \text{Le} = \left(\frac{v}{D_i}\right)\left(\frac{a}{v}\right) \Rightarrow \text{Le} = \frac{a}{D_i} \tag{69}$$

According to Eq.(69) and the above assumptions, the ratio of Sherwood and Nusselt numbers is defined as follows

$$\frac{\text{Sh}}{\text{Nu}} = a_4 \text{Ta}_m{}^{b_4} \text{Le}^{0.33} \tag{70}$$

The enhancement effect of the solid dissolution process due to heat transfer process obtained from Eq.(70) is given by

$$\left(\frac{\beta_i d_s}{D_i}\right)\left(\frac{\lambda}{\alpha_s D}\right) = a_4 \text{Ta}_m{}^{b_4} \text{Le}^{0.33} \tag{71}$$

The ratio $\left(\dfrac{\beta_i}{\alpha_s}\right)$ may be defined by means of the following relationship

$$\left(\frac{\beta_i}{\alpha_s}\right) = a_4 \text{Ta}_m{}^{b_4} \text{Le}^{0.33} \left(\frac{D}{d_s}\right)\left(\frac{D_i}{\lambda}\right) \tag{72}$$

Introducing the thermal diffusivity $\left(a = \dfrac{\lambda}{c_p \rho} \Rightarrow \lambda = a c_p \rho\right)$ in Eq.(72), gives the relation

$$\left(\frac{\beta_i}{\alpha_s}\right) = a_4 \text{Ta}_m{}^{b_4} \text{Le}^{0.33}\left(\frac{D_i}{a}\right)\left(\frac{1}{c_p \rho}\right)\left(\frac{D}{d_s}\right) \Rightarrow \left(\frac{\beta_i}{\alpha_s}\right) = a_4 \text{Ta}_m{}^{b_4} \text{Le}^{0.33} \text{Le}^{-1}\left(\frac{1}{c_p \rho}\right)\left(\frac{D}{d_s}\right) \tag{73}$$

Finally, form relation (73) it follows that

$$\left(\frac{\beta_i}{\alpha_s}\right) = a_4 \mathrm{Ta}_m^{\ b_4} \mathrm{Le}^{-0.66} \left(\frac{1}{c_p \rho}\right)\left(\frac{D}{d_s}\right) \tag{74}$$

3. Experimental details

3.1. Experimental set-up

All experimental measurements of mass-transfer process using the TRMF were carried out in a laboratory set-up including electromagnetic field generator. A schematic of the experimental apparatus is presented in figure 1.
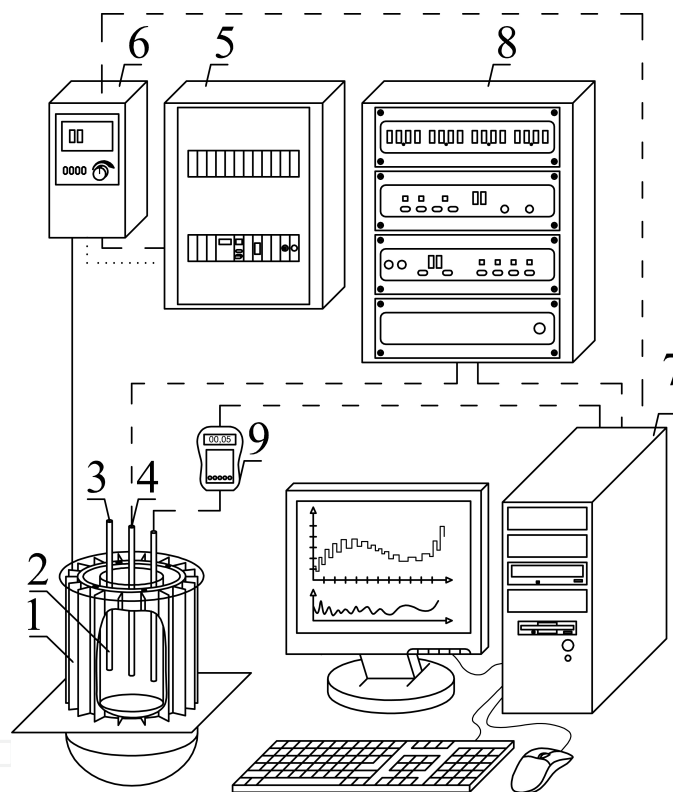

Figure 1. Sketch of experimental set-up: 1 - generator of rotating magnetic field, 2 - glass container, 3,4 - conductivity samples, 5 - electronic control box, 6 - a.c. transistorized inverter, 7 - personal computer, 8 - multifunctional electronic switch, 9 - Hall sample

This setup may be divided into: a generator of the rotating electromagnetic field (1), a glass container (2) with the conductivity samples (3-4), an electric control box (5) and an inverter (6) connected with multifunctional electronic switch (8) and a personal computer (7) loaded with special software. This software made possible the electromagnetic field rotation control, recording working parameters of the generator and various state parameters.

From preliminary tests of the experimental apparatus, the glass container is not influenced by the working parameters of the stator. The TRMF was generated by a modified 3-phase

stator of an induction squirrel-cage motor, parameters of which are in accordance with the Polish Standard PN-72/E-06000. The stator is supplied with a 50 Hz three-phase alternating current. The transistorized inverter (4) was used to change the frequency of the rotating magnetic field in the range of $f_{TRMF} = 1 - 50 Hz$. The stator of the electric machine, as the RMF generator is made up of a number of stampings with slots to carry the three phase winding. The number of pair poles per phase winding, p, is equal to 2. The windings are geometrically spaced 120 degrees apart. The stator and the liquid may be treated as apparent virtual electrical circuit of the closed flux of a magnetic induction. The stator windings are connected through the a.c. transistorized inverter to the power source. The generator produces an azimuthal electromagnetic force in the bulk of the TRMF reactor with the magnetic field lines rotating in the horizontal plane.

For the experimental measurements, MF is generated by coils located axially around of the cylindrical container. As mentioned above, this field is rotated around the container with the constant angular frequency, ω_{TRMF}. The TRMF strength is determined by measuring a magnetic induction. The values of the magnetic induction at different points inside the glass container are detected by using a Hall sample connected to the personal computer. The typical example of the dependence between the spatial distributions of magnetic induction and the various values of the alternating current frequency for the cross-section of container is given [20]. The obtained results in this paper suggest that the averaged values of magnetic induction may be analytically described by the following relation

$$\left[B_{TRMF} \right]_{avg} = 14.05 \left[1 - \exp\left(-0.05 f_{TRMF} \right) \right]$$ (75)

3.2. Rock-salt sample

Two conductive samples connected to a multifunction computer meter were used to measuring and recording of the concentration of the achieve solution of the salt. The mass of the rock salt sample decreasing during the process of dissolution is determined by an electronic balance that connected with rocking double-arm lever. On the lever arm the sample was hanging, the other arm connected to the balance. In the present investigation the change in mass of solid body in a short time period of dissolution is very small and the mean area of dissolved cylinder of the rock salt may be used. Than the mean mass-transfer Raw rock-salt (>98% NaCl and rest traces quantitative of chloride of K, Ca, Mg and insoluble mineral impurities) cylinders were not fit directly for the experiments because their structure was not homogeneous (certain porosity). Basic requirement concerning the experiments was creating possibly homogeneous transport conditions of mass on whole interfacial surface, which was the active surface of the solid body. These requirements were met thanks to proper preparing of the sample, mounting it in the mixer and matching proper time of dissolving. As an evident effect were fast showing big pinholes on the surface of the dissolved sample as results of local non-homogeneous of material. Departure from the shape of a simple geometrical body made it impossible to take measurements of its area with sufficient precision. So it was necessary to put those samples through the process of so-called hardening. The turned

cylinders had been soaked in saturated brine solution for about 15 min and than dried in a room temperature. This process was repeated four times. To help mount the sample in the mixer, a thin copper thread was glued into the sample's axis. The processing was finished with additional smoothing of the surface with fine-grained abrasive paper. A sample prepared in this way had been keeping its shape during dissolving for about 30 min. The duration of a run was usually 30 sec. The rate of mass-transfer involved did not produce significant dimensional change in diameter of the cylinder. The time of a single dissolving cycle was chosen so that the measurement of mass loss could be made with sufficient accuracy and the decrease of dimensions would be relatively small (maximum about 0.5 mm).
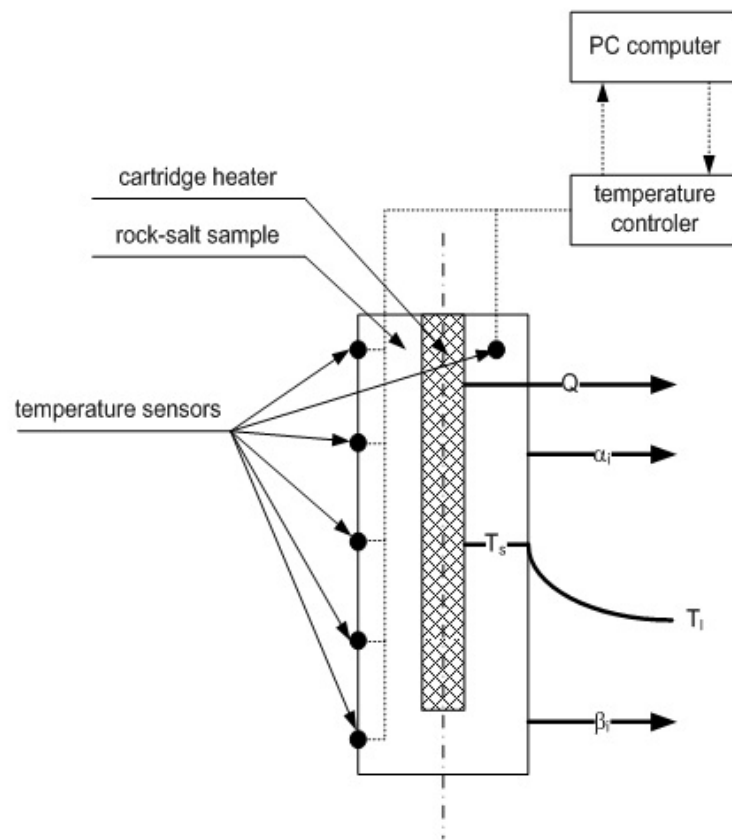

Figure 2. Sketch of rock-salt sample with the heating set-up

Before starting every experiment, a sample which height, diameter and mass had been known was mounted in a mixer under the free surface of the mixed liquid. The reciprocating plate agitator was started, the recording of concentration changes in time, the weight showing changes in sample's mass during the process of solution, and time measuring was started simultaneously. After finishing the cycle of dissolving, the agitator was stopped, and then the loss of mass had been read on electronic scale and concentration of NaCl (electrical conductivity) in the mixer as well. This connection is given by a calibration curve, showing the dependence of the relative mass concentration of NaCl on the electrical conductivity [21].

3.3. Rock-salt sample heated by means of the cartridge heater

In the case of this experimental investigations the gradient temperature between the surface and liquid was caused by using the cartridge heater (power ~1200W). This tubular device was inserted into drilled holes of rock-salt sample for heating. Moreover, the heating set-up was contained the temperature controller and sensors. The sensors for the temperature control was placed between the working surface of the sample and the heater. These sensors was also located on the surface of the solid sample. The sketch of rock-salt sample with the heating set-up is graphically presented in figure 2. The sample was kept at a constant temperature (65°C, 70°C or 80°C). The heat transfer from the sample to ambient fluid was realized for the various temperature (20°C, 40°C and 60°C). The system of temperature sensors was used to control the temperature of the water during the solid dissolution process.

3.4. Experimental calculation of mass transfer coefficient

The mass transfer coefficient under the action of TRMF may be calculated form the following equation

$$-\frac{dm_i}{d\tau} = \beta_i F_m \, \tilde{c}_i \Rightarrow \beta_i = \frac{1}{F_m\left(-\tilde{c}_i\right)} \frac{dm_i}{d\tau} \tag{76}$$

The above Eq.(76) cannot be integrated because the area of solid body, F_m, is changing in time of dissolving process. It should be noted that the change in mass of solid body in a short time period of dissolving is very small and the mean area of dissolved cylinder may be used. The relation between loss of mass, mean area of mass-transfer and the mean driving force of this process for the time of dissolving duration is approximately linear and then the mass-transfer coefficient may be calculated from the simple linear equation

$$\left[\beta_i\right]_{avg} = \frac{1}{\left[F_m\right]_{avg}\left[\tilde{c}_i\right]_{avg}} \frac{\left(-dif\,m_i\right)}{\left(dif\,\tau\right)} \tag{77}$$

The averaged surface F_m is defined as follows

$$\left[F_m\right]_{avg} = \pi\left[d_s\right]_{avg} h_s \tag{78}$$

The volumetric mass transfer coefficient $\left(\beta_i\right)_V$ in Eq.(48) is described by relation

$$\left(\beta_i\right)_V = \frac{\beta_i dF_m}{dV} \Rightarrow \left[\left(\beta_i\right)_V\right]_{avg} = \frac{\left[\beta_i\right]_{\alpha}\left[F_m\right]_{r}}{V_l} \tag{79}$$

3.5. Experimental calculation of heat transfer coefficient

The heat transfer from the sample to liquid may by modelled by the following relationship

$$Q_s = Q_l \Rightarrow \alpha_s F_m \Delta T_1 = m_l c_{p_l} \Delta T_2 \tag{80}$$

This equation can be rewritten as

$$\alpha_s F_m \left(T_s - [T_l]_{t_2} \right) = m_l c_{p_l} \left([T_l]_{t_2} - [T_l]_{t_1} \right) \Rightarrow \alpha_s = \frac{m_l c_{p_l} \left([T_l]_{t_2} - [T_l]_{t_1} \right)}{F_m \left(T_s - [T_l]_{t_2} \right)} \tag{81}$$

and the averaged heat transfer coefficient is given as follows

$$[\alpha_s]_{avg} = \frac{m_l [c_{p_l}]_{avg} \left([T_l]_{t_2} - [T_l]_{t_1} \right)}{[F_m]_{avg} \left(T_s - [T_l]_{t_2} \right)} \tag{82}$$

The averaged coefficient of heat transfer $\left([\alpha_s]_{avg} \right)$ varies with the parameters of the TRMF mixing process and depends on the operating conditions and physical properties of the liquid.

4. Results and discussion

Under the TRMF conditions a relationship for the mass-transfer can be described in the general form $Sh = f\left(Ta_m, Sc \right)$. The results of experiments suggest that the Sherwood number, the magnetic Taylor number and the Schmidt number may be defined as follows (see Eqs 53-56)

$$Sh = \frac{\left[(\beta_i)_V \right]_0 d_p^2}{\rho_0 D_{i_0}} \Rightarrow Sh = \frac{\left(\frac{[\beta_i]_{\alpha} [F_m]_{\alpha}}{V_l} \right) d_p^2}{\rho_l D_{i_l}} \tag{83}$$

$$Sc_i = \frac{\nu}{D_{i_0}} \Rightarrow Sc_i = \frac{\nu_l}{D_{i_l}} \tag{84}$$

$$\text{Ta}_m = \text{Ha}^2 \, \text{Re}_m \Rightarrow \text{Ta}_m = \left(\frac{\sigma_{e_0} B_0^2 l_0^2}{\nu \rho_0}\right)\left(\frac{w_0 D}{\nu}\right) \Rightarrow \text{Ta}_m = \left(\frac{\sigma_{e_l} \left([B_{TRMF}]_{avg}\right)^2 D^2}{\nu_l \rho_l}\right)\left(\frac{\omega_{TRMF} D^2}{\nu_l}\right)$$

$$\Rightarrow \text{Ta}_m = \frac{\omega_{TRMF}\left([B_{TRMF}]_{avg}\right)^2 D^4 \sigma_{e_l}}{\nu_l^2 \rho_l}$$

(85)

The TRMF Reynolds number $\left(\text{Re}_m = \dfrac{\omega_{TRMF} D^2}{\nu_l}\right)$ with $\omega_{TRMF} = 2\pi f_{TRMF}$ as angular frequency of TRMF equal to angular field frequency of the field generated by the a current of frequency. The product $\omega_{TRMF} D$ plays the role of a rotational velocity. The above dimensionless groups (Eqs 83-85) were calculated with the physical properties in the temperature range 20-60°C (the liquid temperature).

The effect of dissolution process under the action of TRF can be described by using the variable $\text{ShSc}^{-0.33}$ proportional to the term $a(Ta_m)^b$. The experimental results obtained in this work are graphically illustrated in $\log(\text{ShSc}^{-0.33})$ versus $\log(a(Ta_m)^b)$ in figure 3. Moreover, the influence of the temperature gradient between the surface temperature of solid and the liquid temperature on the mass transfer coefficient is presented in this figure.

In order to establish the effect of all important parameters on the dissolution process in the analyzed set-up, we propose the following relationship to work out the experimental database

$$\frac{\text{Sh}}{\text{Sc}^{0.33}} = a\left(\text{Ta}_m\right)^b$$

(86)

The presented results in figure 3 suggest that these points may be described by a unique monotonic function. The constants and exponents are computed by employing the Matlab software and the principle of least squares and the proposed relationships are collected in table 1.

Figure 4 shows the effect of the constant temperature of the surface of rock-salt sample and the variation of the liquid temperature on the Sherwood number.

temperature of surface of salt-rock sample	temperature of liquid		
	20°C	40°C	60°C
65°C	$\frac{\text{Sh}}{\text{Sc}^{0.33}} = 80.36\left(\text{Ta}_m\right)^{0.146}$	$\frac{\text{Sh}}{\text{Sc}^{0.33}} = 79.71\left(\text{Ta}_m\right)^{0.08}$	$\frac{\text{Sh}}{\text{Sc}^{0.33}} = 51.95\left(\text{Ta}_m\right)^{0.06}$
70°C	$\frac{\text{Sh}}{\text{Sc}^{0.33}} = 85.54\left(\text{Ta}_m\right)^{0.132}$	$\frac{\text{Sh}}{\text{Sc}^{0.33}} = 84.13\left(\text{Ta}_m\right)^{0.05}$	$\frac{\text{Sh}}{\text{Sc}^{0.33}} = 67.52\left(\text{Ta}_m\right)^{0.04}$
80°C	$\frac{\text{Sh}}{\text{Sc}^{0.33}} = 92.87\left(\text{Ta}_m\right)^{0.09}$	$\frac{\text{Sh}}{\text{Sc}^{0.33}} = 92.85\left(\text{Ta}_m\right)^{0.04}$	$\frac{\text{Sh}}{\text{Sc}^{0.33}} = 73.71\left(\text{Ta}_m\right)^{0.03}$

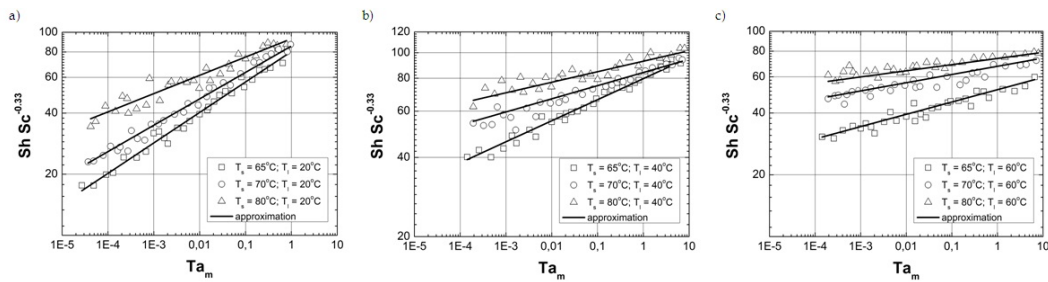**Table 1.** The developed relationships for the obtained experimental data

Figure 3. The graphical presentation of mass transfer data under the action of TRMF: a)T_s=var;T_l=20°C, b) T_s=var;T_l=40°C and c) T_s=var;T_l=60°C
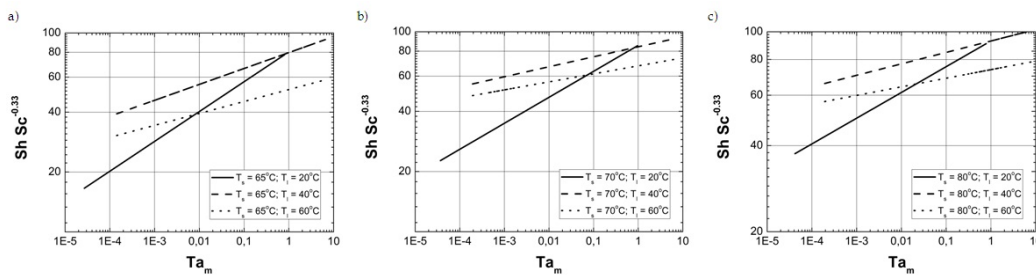
Figure 4. The comparison of obtained results: : a)T_s=65°C;T_l=var, b) T_s=70°C;T_l=var and c) T_s=80°C;T_l=var

Figures 3 and 4 present a graphical form of the collected relations in table 1, as the full curves, correlated the experimental data very well with the percentage relative error±10%. Figure 5 gives an overview results in the form of the proposed analytical relationships for the experimental investigations (see table 1)
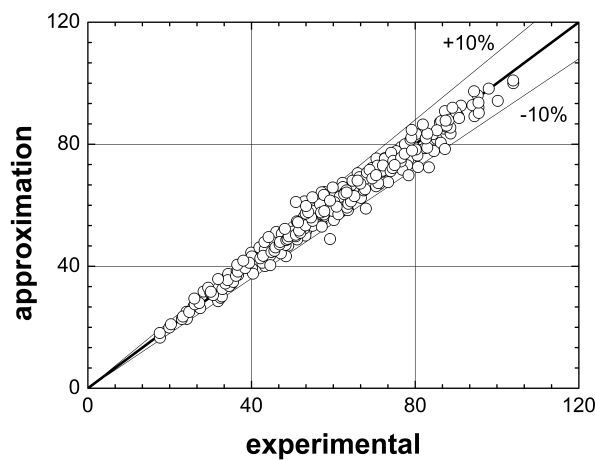

Figure 5. Dependence between experimental and predicted $\left(\dfrac{Sh}{Sc^{0.33}}\right)$ values

As can be clearly seen (see Figure 3) mass transfer rates expressed as $\left(\dfrac{Sh}{Sc^{0.33}}\right)$ increase with increasing the values of magnetic Taylor number. It is found that as the intensity of magnetic field increases, the velocity of liquid inside the cylindrical container increases. It may be concluded that the TRMF strongly influenced on the mass transfer process. It should be noticed that this process may be improved by means of the gradient temperature between the surface of rock-salt sample and the liquid. Figure 3 shows that Sherwood number increases with the increasing difference between the temperature of rock-salt surface and the liquid temperature. It is clear that the effect of TRMF on the dissolution process is also depended on the temperature gradient.

Comparison of the obtained results for the analyzed process is graphically presented in figure 4. This figure shows that for the given temperature of surface of rock-salt sample the mass transfer coefficients in tested set-up are strongly depended on the values of magnetic Taylor number. These plots also confirm that the gradient temperature has significant effect on the mass transfer process. Initially, the high mass transfer rates is achieved by the liquid temperature 40°C and 60°C. Further increase of the magnetic field intensity leads to even higher mass transfer rates for the liquid temperature is equal to 20°C. It should be noticed that the NaCl-cylinder was placed in the middle of container. When the TRMF rotated slowly the liquid was mixed near the wall of cylindrical container. When the TRMF rotated faster, the resulting liquid movement directly leads to an increase of the mass and heat transfer coefficients. This difference appears to be linked to the increase in the difference between the surface temperature of rock-salt sample and the liquid temperature associated with increasing the influence of TRMF. The high value of the exponents of magnetic Taylor number and the multiplicative coefficients seen in the relations given in table 1 agree with the existence of more intensive flow near the hot surface of the rock-salt sample promoted by the increase of the magnetic induction and the temperature of the cartridge heater.
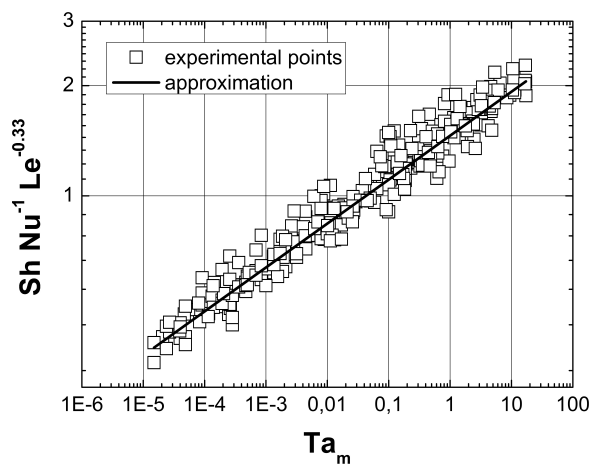

Figure 6. The graphical presentation of mass and heat transfer data at TRMF

The enhancement due to heat transfer process is modeled in terms given in Eq.(70). The graphical presentation of the calculated experimental points is presented in figure 6.

The constant a_4 and exponent b_4 in Eq.(70) are computed by using the principle of least square. Applying the software Matlab the analytical relationship may be obtained

$$\frac{Sh}{Nu} = 1.5\left(Ta_m\right)^{0.12} Le^{0.33} \tag{87}$$

where the ratio of the dimensionless Sherwood and Nusselt numbers is function of the adequate dimensionless groups. The fit of experimental data with Eq.(87) is given in figure 7. The averaged absolute relative error was estimated at 2.12%.
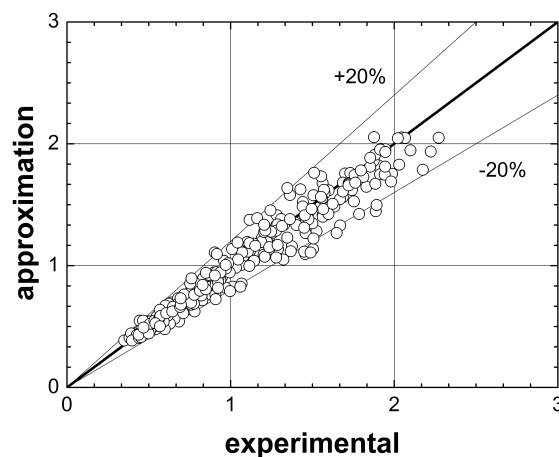

Figure 7. Comparison of model prediction (Eq.(87)) with experimental data

Figure 6 shows that the ratio of mass and heat transfer coefficients (via ratio of Sherwood and Nusselt numbers) increases with the magnetic Taylor number. This figure shows a strong increase in mass transfer process when the TRMF is applied. It was found that the intensification of this process is depended on the temperature gradient between the temperature of surface of salt-rock sample and the liquid temperature.

In order to evaluate the influence of the gradient temperature on the mass transfer under the action of TRMF, the comparison between the obtained database and the empirical correlation for the dissolution process under the TRMF is presented. For comparison these results with literature, it is recommended to correlate them under analogous form. The dissolution process under the action of TRMF is correlated by means of the equation [22]

$$Sh = 2 + 22.5\{Ta_m\}_x^{0.015} Sc^{0.33}\left(\frac{x}{D}\right)^{0.33} \tag{88}$$

Taking into account that the dimensionless location of a NaCl-cylindrical sample $\left(\dfrac{x}{D}\right)$ is equal to 0.125 (the sample was located in the middle of cylindrical container) and the local Taylor number $\left(\{Ta_m\}_x\right)$ is treated as the magnetic Taylor number (Ta_m), the Eq.(88) may be rewritten in the following form

$$Sh = 2 + 11.3\{Ta_m\}_x^{0.015} Sc^{0.33} \Rightarrow Sh_I = 2 + 11.3(Ta_m)^{0.015} Sc^{0.33} \tag{89}$$

As a matter of fact, Eq.(70) may be written by alternate equations as follows

$$Sh_{II} = 1.5(Ta_m)^{0.12} Le^{0.33} Nu \tag{90}$$

The comparison in this case may be realized by considering the calculated averaged values of the dimensionless Schmidt $([Sc]_{avg}=477)$, Lewis $([Le]_{avg}=74)$ and Nusselt $([Nu]_{avg}=102)$ numbers. For established averaged values of these dimensionless groups the Eqs (89-90) reduce to

$$Sh_I = 2 + 86.5(Ta_m)^{0.015} \tag{91}$$

$$Sh_{II} = 616.3(Ta_m)^{0.12} \tag{92}$$

The graphical comparison between Eq.(91) and Eq.(92) are illustrated in the plot in figure 8. This figure demonstrates that the dimensionless Sherwood number for the analyzed case (Sh_{II}) increases with increasing the magnetic Taylor number. It was found that as the intensity of TRMF increases, the influence of hydrodynamic conditions on the transport processes inside the cylindrical container increases. The obtained relationship (Eqs (91-92)) indicate that the transfer rates increase with Taylor number for case I $Sh_I \sim (Ta_m)^{0.015}$ and case II $Sh_{II} \sim (Ta_m)^{0.12}$. The mass transfer data obtained for the additional transfer gradient is consequently higher than the data obtained for the mass transfer under the action of TRMF.

It can be observed that the enhancement of the mass transfer coefficients due to temperature gradient may be evaluated by applying the ratio $\left(\dfrac{Sh_{II}}{Sh_I}\right)$. In the present study $\left(\dfrac{Sh_{II}}{Sh_I}\right)$ becomes

$$\left(\frac{Sh_{II}}{Sh_I}\right) = \frac{616.3(Ta_m)^{0.12}}{2 + 86.5(Ta_m)^{0.015}} \Rightarrow \left(\frac{Sh_{II}}{Sh_I}\right) \approx 5(Ta_m)^{0.105} \tag{93}$$

Figure 9 shows the obtained relation (see Eq.(93)) as the function of the magnetic Taylor number. It was found that as the intensity of TRMF has strong influence on the mass transfer rate. It is interesting to note that the enhancement of this process in the case of upper values of the magnetic Taylor number is increased for the supported process by using the cartrige heater.
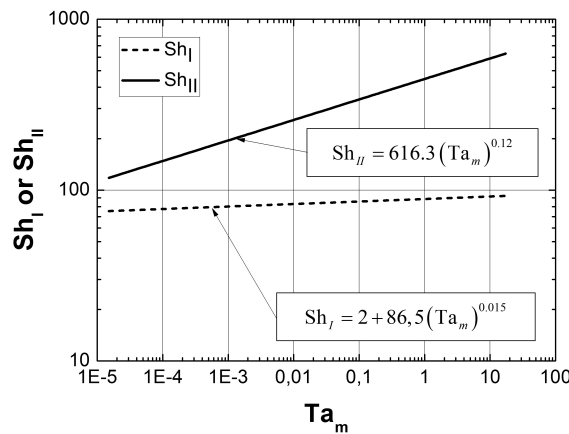

Figure 8. Comparison of obtained results $\left(Sh_{II}\right)$ with literature data $\left(Sh_{I}\right)$
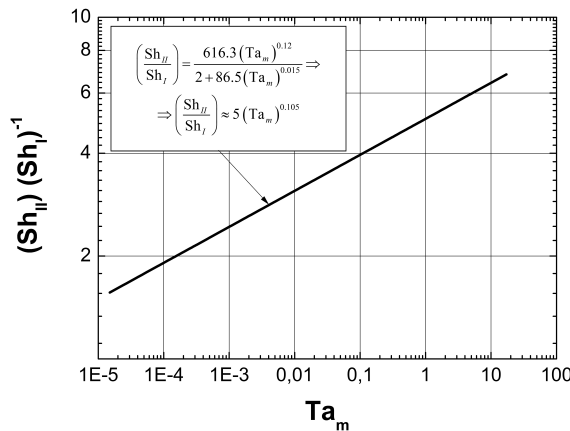

Figure 9. Graphical presentation of Eq.(93)

5. Conclusion

The present experimental study shows interestingfeatures cocncerning the effects of transverse rotating magnetic field (TRMF) on the mass transfer process. Inspecting the obtained measuremenst reveals the following conclusions:

1. The study of mass transfer process under the action of TRMF results is significant en-hancement of the solid dissolution rate per localization of a NaCl-cylindrical sample. The mass transfer rate increases with an increase of a magnetic field level. It was found that the TRMF strongly influcnecd the mass transfer process.

2. It should be noticed that the novel approach to the mixing process presented and based on the application of TRMF to produce better hydrodynamic conditions in the case of the mass-transfer process. From practical point of view, the dissolution process of solid body is involved by using the turbulently agitated systems. In previous publications are not available data describing the mass-transfer operations of the dissolution process un-der the TRMF conditions and the temperature gradient. Moreover, the influence of the additional indirect heating on the mass-transfer was determined.

3. With the respect to the other very useful mass transfer equations given in the pertinent literature, the theoretical description of problem and the equations predicted in the present article is much more attractive because it generalizes the experimental data tak-ing into consideration the various parameters, which defined the hydrodynamic state and the intensity of magnetic effects in the tested system (see chapter 2.2).

4. On the basis of the experimental investigations, the results were successfully correlated by using the general relationship [74]. The influence of the TRMF and the temperature gradient on this process may be also described using the non-dimensional parameters formulated on the base of fluid mechanics equations. These dimensionless numbers al-low quantitative representation and characterization of the influence of hydrodynamic state under the TRMF conditions on the mass-transfer process. The dimensionless groups are used to establish the effect of TRMF on this operation in the form of the nov-el type dimensionless correlation [87].

5. In order to evaluate the influence of the gradient temperature on the mass transfer un-der the action of TRMF, the comparison between the obtained database and the empiri-cal correlation for the dissolution process under the TRMF is presented. This coparsion is presented as the specific relation [93]. It can be observed that the enhancement of the mass transfer coefficients due to temperature has strong influence on the mass transfer rate (see Fig.8).

6. Nomenclature

$\bar{B}$	magnetic induction	$kg \cdot A^{-1} \cdot s^{-2}$
c_i	concentration	$kg_i \cdot kg^{-1}$
c_p	specific heat capacity of liquid	$J \cdot kg^{-1} \cdot deg^{-1}$
d_s	sample diameter	m

D	diameter of container	m
D_i	diffusion coefficient	$m^2 \cdot s^{-1}$
D_m	magnetic diffusion	$m^2 \cdot s^{-1}$
$\bar{E}$	electric field	$V \cdot m^{-1}$
f_{TRMF}	frequency of electrical current (equal to frequency of TRMF)	s^{-1}
F_m	cylindrical surface of dissoluble sample	m^2
$\overline{F_{em}}$	Lorenz magnetic force	N
h_s	length of sample	m
l	characteristic dimension	m
$\bar{J}$	electrical current density vector	$A \cdot m^{-2}$
$\bar{J}_i$	flux density of component i	$kg_i \cdot m^{-3} \cdot s^{-1}$
$\overline{J_{dyf}}$	diffusion flux density	$kg_i \cdot m^{-3} \cdot s^{-1}$
k_p	relative coefficient of barodiffusion	$kg_i \cdot m^2 \cdot kg^{-1} \cdot N^{-1}$ $\left(kg_i \cdot m \cdot s^2 \cdot kg^{-2} \right)$
k_p	relative coefficient of thermodiffusion	$kg_i \cdot kg^{-1} \cdot \deg^{-1}$
$k_{\overline{F_{em}}}$	relative coefficient of diffusion resulting from additional forced interactions (e.g. magnetic field)	$kg_i \cdot m^{-1} \cdot N^{-1}$ $\left(kg_i \cdot s^2 \cdot m^{-2} \cdot kg^{-1} \right)$
m_i	mass of dissoluble NaCl sample	kg_{NaCl}
p	hydrodynamic pressure	$N \cdot m^{-2}$
Q_l	heat flow from liquid	W
Q_s	heat flow from sample	W
S	shielding parameter	-
T	temperature	deg
$[T_l]_{t_1}$	temperature of liquid at moment t_1	deg
$[T_l]_{t_2}$	temperature of liquid at moment t_2 (after time of dissolution process)	deg
T_s	temperature of sample	deg
V	volume of liquid	m^3
$\bar{w}$	velocity	$m \cdot s^{-1}$
$\bar{w}_i$	velocity of component i	$m \cdot s^{-1}$
x	distance (for localization of sample)	m

Table 2.

α_s	heat transfer coefficient	$W \cdot m^{-2} \cdot deg^{-1}$
β_i	mass transfer coefficient	$kg_i \cdot m^{-2} \cdot s^{-1}$
δ	skin depth	-
η	dynamic viscosity	$kg \cdot m^{-1} \cdot s^{-1}$
μ_m	magnetic permeability	$kg \cdot m \cdot A^{-2} \cdot s^{-2}$
λ	thermal conductivity of liquid	$W \cdot m^{-1} \cdot deg^{-1}$
v	kinematic viscosity	$m^2 \cdot s^{-1}$
v_m	magnetic viscosity	$m^2 \cdot s^{-1}$
ρ	density	$kg \cdot m^{-3}$
ρ_i	concentration of component i	$kg_i \cdot m^{-3}$
σ_e	electrical conductivity	$A^2 \cdot s^3 \cdot kg^{-1} \cdot m^{-3}$
τ	time dissolution or time	s
Φ_i	mass flux of component i	$kg_i \cdot m^{-3} \cdot s^{-1}$
ω_{TRMF}	angular velocity of transverse rotating magnetic field	$rad \cdot s^{-1}$

Greek letters

avg	averaged value
l	liquid
s	sample
0	reference value

Subscripts

AC	alternating current
MF	magnetic field
TRMF	transverse rotating magnetic field

Abbreviation

$Ha = B_0 l_0 \sqrt{\dfrac{\sigma_{e_0}}{v \rho_0}}$	Hartman number

$Le = \dfrac{a}{D_i}$		Lewis number
$Nu = \dfrac{[\alpha_s]_{avg} D}{\lambda}$		Nusselt number
$Pe_i = \dfrac{l_0 w_0}{D_{i_0}}$		mass Peclet number
$Pr_m = \dfrac{\nu}{\nu_{m_0}}$		magnetic Prandtl number
$Q = \dfrac{\sigma_{e_0} B_0^2 l_0^2}{\nu \rho_0}$		Chandrasekhar number
$Re = \dfrac{w_0 D}{\nu}$		Reynols number
$S = \dfrac{\tau_0 w_0}{l_0}$		Strouhal number
$Sc_i = \dfrac{\nu}{D_{i_0}}$		Schmidt number
$Sh = \dfrac{[(\beta_i)_V]_0 d_p^2}{\rho_0 D_{i_0}}$		Sherwood number

Dimensionless numbers

Acknowledgements

Author details

Rafał Rakoczy[*], Marian Kordas and Stanisław Masiuk

*Address all correspondence to: rrakoczy@zut.edu.pl

Institute of Chemical Engineering and Environmental Protection Process, West Pomeranian University of Technology, Poland

References

[1] Aksielrud, G. A., & Mołczanow, A. D. (1981). *Dissolution process of solid bodies*, WNT Poland (in polish).

[2] Al-Qodah, Z., Al-Bisoul, M., & Al-Hassan, M. (2001). Hydro-thermal behavior of magnetically stabilized fluidized beds. *Powder Technology*, 115, 58-67.

[3] Basmadjian, D. (2004). *Mass transferPrinciples and applications* CRC Press LLC, USA.

[4] Bird, R. B., Stewart, W. E., & Lightfoot, E. N. (1966). *Transport phenomena*, Wiley, USA.

[5] Condoret, J. S., Riba, J. P., & Angelino, H. (1989). Mass transfer in a particle bed with oscillating flow. *Chemical Engineering Science*, 44(10), 2107-2111.

[6] Fraňa, K., Stiller, J., & Grundmann, R. (2006). Transitional and turbulent flows driven by a rotating magnetic field. *Magnetohydrodynamics*, 42, 187-197.

[7] Garner, F. H., & Suckling, R. D. (1958). Mass transfer form a soluble solid sphere. *AIChE Journal*, 4(1), 114-124.

[8] Guru, B. S., & Hiziroğlu, H. R. (2004). *Electromagnetic field theory fundamentals*, Cambridge University Press.

[9] Hristov, J. (2003). Magnetic field assisted fluidization- A unified approach. Part 3: Heat transfer in gas-solid fluidized beds- a critical re-evaluation of the results. [a], *Reviews in Chemical Engineering*, 19(3), 229-355.

[10] Hristov, J. (2003). Magnetic field assisted fluidization- A unified approach. Part 7: Mass Transfer: Chemical reactors, basic studies and practical implementations thereof. [b], *Reviews in Chemical Engineering*, 25(1-3), 1-254.

[11] Incropera, F. P., & De Witt, D. P. (1996). Fundamentals of heat and mass transfer. John Wiley & Sons Inc., USA.

[12] Jameson, G. J. (1964). Mass (or heat) transfer form an oscillating cylinder. *Chemical Engineering Science*, 19, 793-800.

[13] Kays, W. M., & Crawford, M. E. (1980). Convective heat and mass transfer. McGraw-Hill, USA.

[14] Lemcoff, N. O., & Jameson, G. J. (1975). Solid-liquid mass transfer in a resonant bubble contractor. *Chemical Engineering Science*, 30, 363-367.

[15] Lemlich, R., & Levy, M. R. (1961). The effect of vibration on natural convective mass transfer. *AIChE Journal*, 7, 240-241.

[16] Melle, S., Calderon, O. G., Fuller, G. G., & Rubio, M. A. (2002). Polarizable particle aggregation under rotating magnetic fields using scattering dichroism. *Journal of Colloid and Interface Science*, 247, 200-209.

[17] Mößner, R., & Gerbeth, G. (1999). Buoyant melt flows under the influence of steady and rotating magnetic fields. *Journal of Crystal Growth*, 197, 341-345.

[18] Nikrityuk, P. A., Eckert, K., & Grundmann, R. (2006). A numerical study of unidirectional solidification of a binary metal alloy under influence of a rotating magnetic field. *International Journal of Heat and Mass Transfer*, 49, 1501-1515.

[19] Noordsij, P., & Rotte, J. W. (1967). Mass transfer coefficients to a rotating and to a vibrating sphere. *Chemical Engineering Science*, 22, 1475-1481.

[20] Rakoczy, R., & Masiuk, S. (2009). Experimental study of bubble size distribution in a liquid column exposed to a rotating magnetic field. *Chemical Engineering and Processing: Process Intensification*, 48, 1229-1240.

[21] Rakoczy, R., & Masiuk, S. (2010). Influence of transverse rotating magnetic field on enhancement of solid dissolution process. *AIChE Journal*, 56, 1416-1433.

[22] Rakoczy, R. (2010). Enhancement of solid dissolution process under the influence of rotating magnetic field. *Chemical Engineering and Processing: Process intensification*, 49, 42-50.

[23] Spitzer, K. H. (1999). Application of rotating magnetic field in Czochralski crystal growth. *Crystal Growth and Characterization of Materials*, 38, 39-58.

[24] Sugano, Y., & Rutkowsky, D. A. (1968). Effect of transverse vibration upon the rate of mass transfer for horizontal cylinder. *Chemical Engineering Science*, 23, 707-716.

[25] Tojo, K., Miyanami, K., & Mitsui, H. (1981). Vibratory agitation in solid-liquid mixing. *Chemical Engineering Science*, 36, 279-284.

[26] Volz, M. P., & Mazuruk, K. (1999). Thermoconvective instability in a rotating magnetic field. *International Journal of Heat and Mass Transfer*, 42, 1037-1045.

[27] Walker, J. S., Volz, M. P., & Mazuruk, K. (2004). Rayleigh-Bénard instability in a vertical cylinder with a rotating magnetic field. *International Journal of Heat and Mass Transfer*, 47, 1877-1887.

[28] Wong, P. F. Y., Ko, N. W. M., & Yip, P. C. (1978). Mass transfer from large diameter vibrating cylinder. *Trans. Item*, 56, 214-216.

[29] Yang, M., Ma, N., Bliss, D. F., & Bryant, G. G. (2007). Melt motion during liquid-encapsulated Czochralski crystal growth in steady and rotating magnetic field. *International Journal of Heat and Mass Transfer*, 28, 768-776.